The identification of stacking faults on {1 0 0} and {1 1 0} planes in Pd_3Ce

Although the compound Pd_3Ce is known to possess the Cu_3Au-type structure [1, 2], little is known about its microstructure and no similarities with isostructural compounds such as Ni_3Al or Ni_3Ge have been established. As a first step in the examination of this phase, as-cast material was examined by transmission electron microscopy.

The purest cerium and palladium commercially available were alloyed by arc melting with an argon arc from a tungsten electrode onto a water-cooled copper hearth. 3 mm discs were spark machined from the material thus obtained which were jet-profiled in a 50% hydrochloric acid solution at 80 V and electropolished at 20 V and -10° C in a solution containing 45 vol% glacial acetic acid, 45 vol% 2-*n*-butoxyethanol and 10 vol% perchloric acid. The electron microscopy was performed on Philips EM300 and EM400 microscopes working at 100 kV.

On examination, the material clearly contained a very high density of stacking faults and a number of coarse precipitates (see Fig. 1). Sufficient electron diffraction data to determine the crystal structure of these precipitates was not obtained. However, using the energy dispersive X-ray probe (EDAX) facility on the EM400 electron microscope, the precipitates were found to consist solely of cerium. It therefore seemed likely that the precipitates were cerium oxide since cerium has a high affinity for oxygen and the oxide is known to be the major impurity in commercially available cerium.

Two types of stacking fault were observed, each possessing a quite different distribution. The first type were often as long as 3 μm and were distinctly associated with precipitates. The precipitate marked A in Fig. 1 is a typical example showing faults emanating from both ends. The second type were much smaller and were homogeneously distributed throughout the material, as is evident in Fig. 1. Both types of fault were characterized by determining the fault vector and Burgers vector, using the invisibility criterion, and by determining the fault plane using trace analysis.

The fault labelled A in Fig. 2 has been imaged for different diffraction vectors. It can be seen by following through Fig. 2a to e that although the fault is visible for $[\bar{1}\,\bar{1}\,1]$, $[0\,\bar{2}\,2]$ and $[\bar{2}\,0\,2]$ diffraction vectors, it is invisible for $[\bar{2}\,2\,0]$ and $[2\,0\,0]$ diffraction vectors. This defines the fault vector as $1/n[0\,0\,1]$. The dislocations bounding this fault follow the same contrast behaviour as the fault itself and therefore have a Burgers vector of $1/n[0\,0\,1]$. Trace analysis of this fault using the top fringe and dislocation line defined the fault plane as $(0\,0\,1)$ and the dislocation line direction as $[0\,1\,0]$, hence defining the dislocation character as pure edge. Similar analysis of the other faults lying perpendicular to fault A in Fig. 2 established that they lay on the $(1\,0\,0)$ planes with a $1/n[1\,0\,0]$ fault vector and a pure edge bounding dislocation with a $1/n[1\,0\,0]$ Burgers vector.

The other type of faults were arranged in configurations where three faults in three different planes were joined together along a mutual direction. In Fig. 3 the fault configuration labelled B has been considered. The uppermost fault is visible for $[2\,0\,\bar{2}]$, $[0\,\bar{2}\,0]$ and $[\bar{1}\,\bar{1}\,1]$ diffraction vectors and invisible for $[1\,\bar{1}\,\bar{1}]$ and $[0\,2\,2]$ diffraction vectors. The fault must therefore have a fault vector of $1/n[0\,\bar{1}\,1]$. The dislocation bounding the unattached end of the fault follows the same contrast behaviour and hence has a Burgers vector of $1/n[0\,\bar{1}\,1]$. Trace analysis defined the fault plane as $(0\,\bar{1}\,1)$ and the dislocation line direction as $[0\,1\,1]$, thus defining the dislocation as pure edge in character. The mutual direction was found to be $[1\,1\,1]$. Similar contrast and trace analyses defined the lower fault as having a fault vector of $1/n[\bar{1}\,1\,0]$ with a fault plane of $(\bar{1}\,1\,0)$ and its bounding dislocation was again a pure edge with Burgers vector $1/n[\bar{1}\,1\,0]$. The third fault in this particular configuration became apparent for a beam direction which was not contained in the $[\bar{1}\,0\,1]$ zone and is easily seen in Fig. 3f where the beam direction is $[2\,1\,1]$. This fault was found to lie in the $(\bar{1}\,0\,1)$ plane, have a fault vector and dislocation Burgers vector of $1/n[\bar{1}\,0\,1]$ and again this dislocation was of pure edge character. In Fig. 3f, the upper fault appears to be out of contrast but in fact it is being viewed edge-on in the foil. The overall configuration is illustrated schematically in Fig. 4.

The faults lying on $\{0\,0\,1\}$ planes which are clearly associated with precipitates may be related to a change in composition within the precipitates on cooling. Assuming the precipitates to be cerium

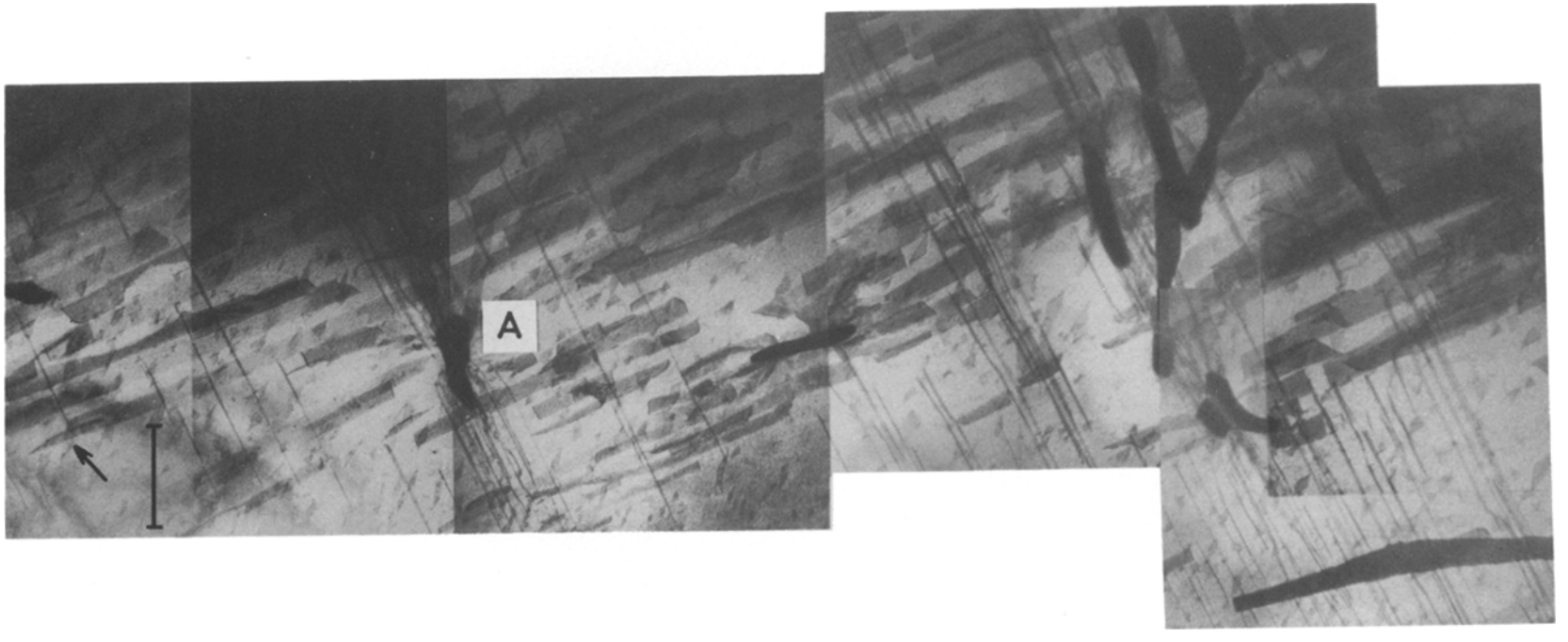

Figure 1 Montage of microstructure showing both types of fault and precipitates. The bar shown corresponds to 1 μm, the beam direction is [165] and the diffraction vector is $[\bar{1}1\bar{1}]$.

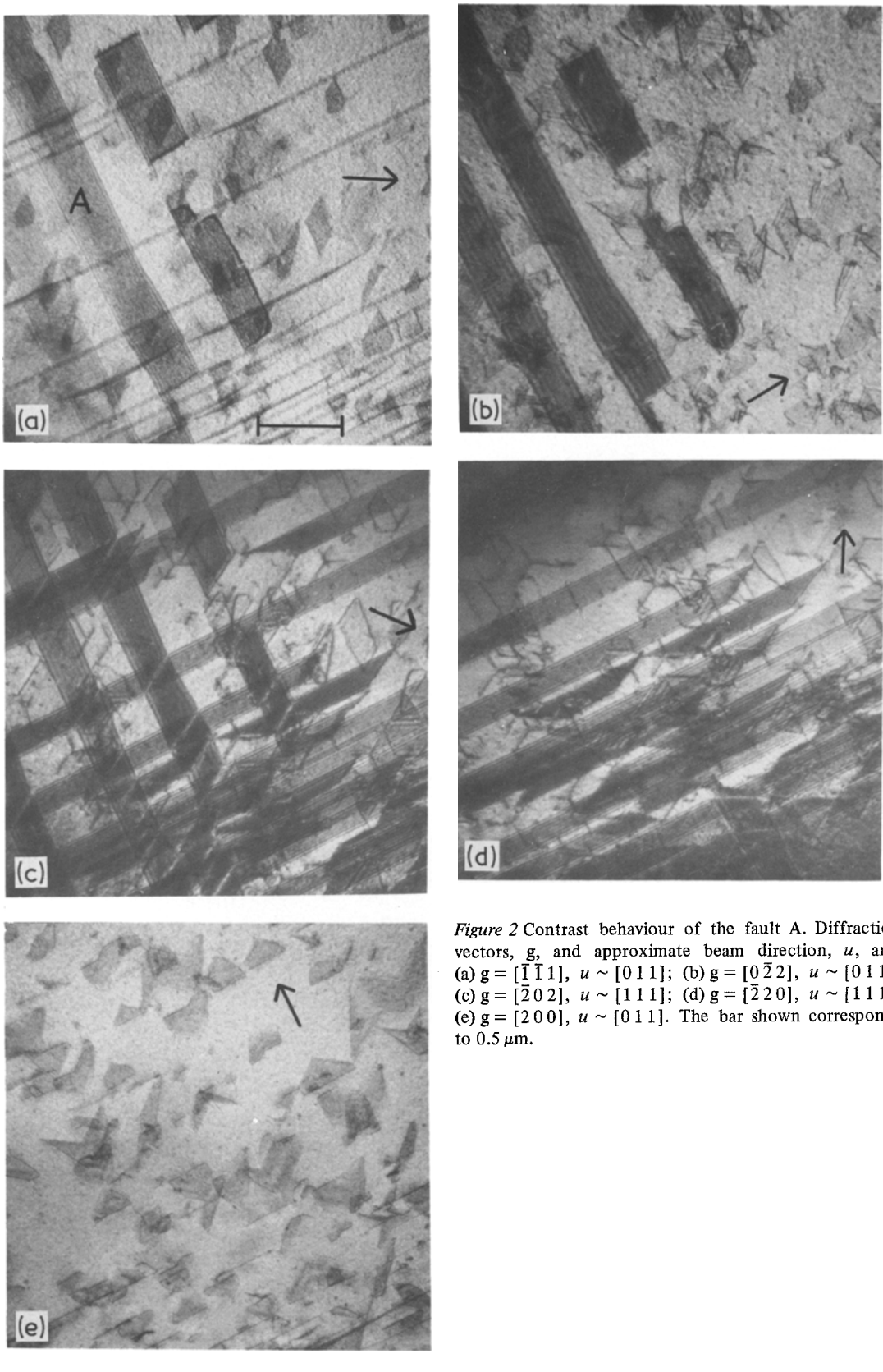

Figure 2 Contrast behaviour of the fault A. Diffraction vectors, g, and approximate beam direction, u, are: (a) $\mathbf{g} = [\bar{1}\,\bar{1}\,1]$, $u \sim [0\,1\,1]$; (b) $\mathbf{g} = [0\,\bar{2}\,2]$, $u \sim [0\,1\,1]$; (c) $\mathbf{g} = [\bar{2}\,0\,2]$, $u \sim [1\,1\,1]$; (d) $\mathbf{g} = [\bar{2}\,2\,0]$, $u \sim [1\,1\,1]$; (e) $\mathbf{g} = [2\,0\,0]$, $u \sim [0\,1\,1]$. The bar shown corresponds to 0.5 μm.

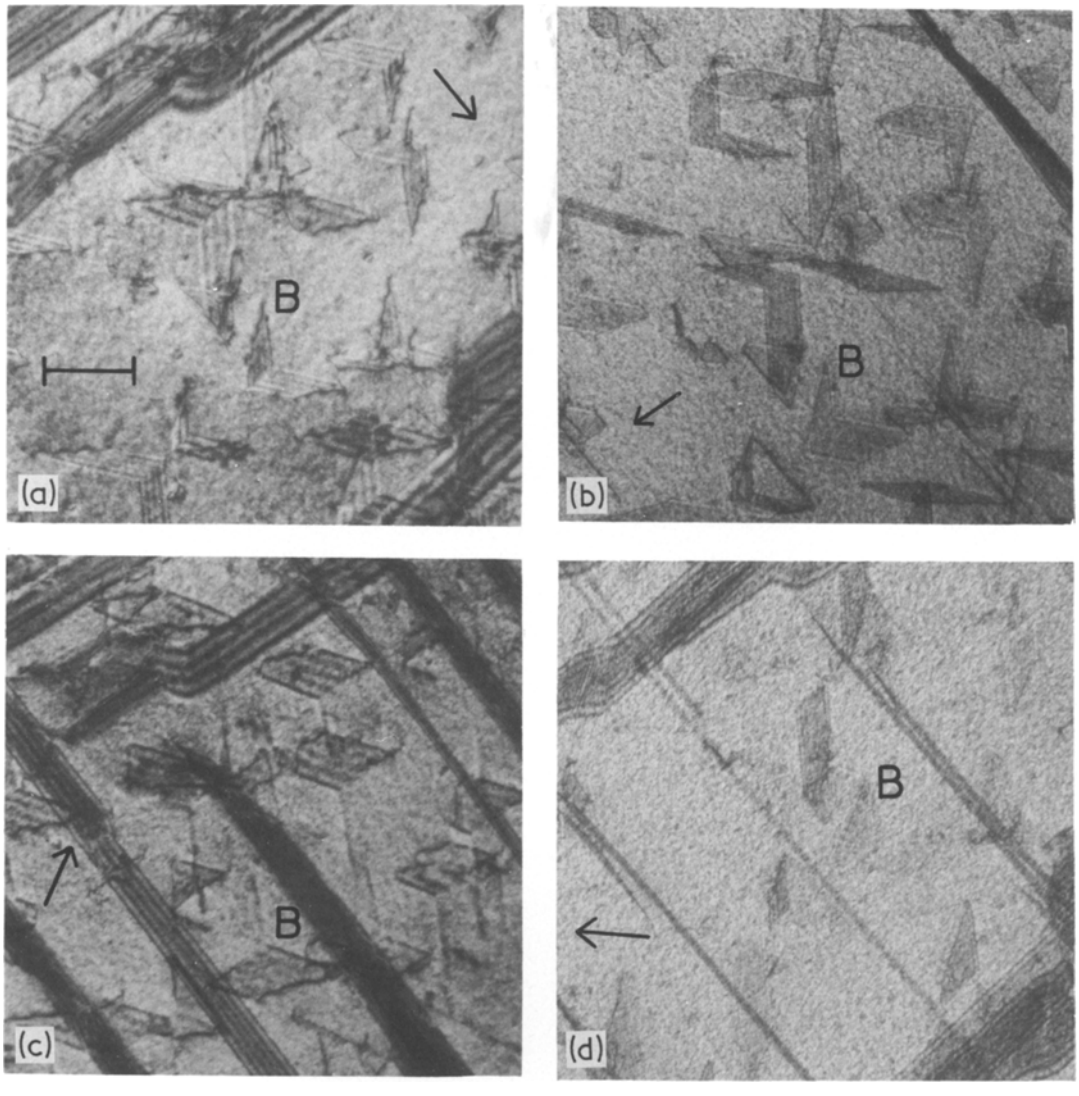

Figure 3 Contrast behaviour of the fault configuration B. Diffraction vectors, **g**, and approximate beam direction, u, are: (a) $\mathbf{g} = [2\,0\,\bar{2}]$, $u \sim [1\,0\,1]$; (b) $\mathbf{g} = [0\,\bar{2}\,0]$, $u \sim [1\,0\,1]$, (c) $\mathbf{g} = [0\,2\,2]$, $u \sim [1\,\bar{1}\,1]$; (d) $\mathbf{g} = [\bar{1}\,\bar{1}\,1]$, $u \sim [1\,0\,1]$; (e) $\mathbf{g} = [1\,\bar{1}\,\bar{1}]$, $u \sim [1\,0\,1]$; (f) $\mathbf{g} = [0\,\bar{2}\,2]$, $u \sim [2\,1\,1]$. The bar shown corresponds to 0.25 μm.

oxide, then it is known that CeO_2 may deviate from stoichiometry under partial pressures of oxygen above 680° C [3–7]. Under lower oxygen partial pressures a compositional change from CeO_2 to CeO_x is possible, where x has a minimum value of 1.72 [6]. It is therefore possible that the faults on the $\{0\,0\,1\}$ planes may be associated with either the injection of oxygen atoms or the removal of cerium atoms from the matrix.

The presence of a significant volume of cerium oxide in the cerium used for the original melt charge means that the resultant alloy must be palladium-rich. It is possible that this deviation from stoichiometry may be accommodated by the excess palladium agglomerating into faulted configurations of the type illustrated in Fig. 4. This would lead to a homogeneous distribution but the reason for the development of such a configuration is unclear.

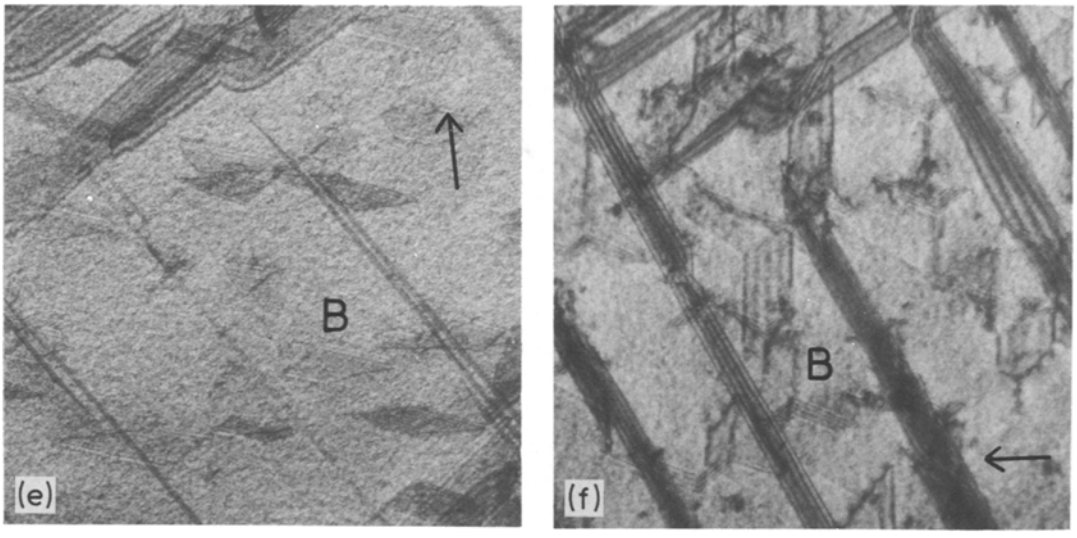

Fig. 3 (Continued)

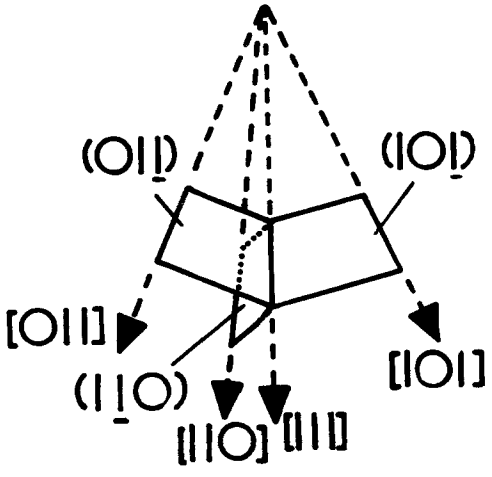

Figure 4 Schematic diagram of the faulted configuration marked B in Fig. 3.

References

1. J. R. THOMPSON, *J. Less-Common Metals* **13** (1967) 307.
2. I. R. HARRIS and M. NORMAN, *ibid.* **15** (1968) 285.
3. D. J. M. BEVAN, *J. Inorg. Nucl. Chem.* **1** (1955) 49.
4. G. BRAUER and K. A. GINGERICH, *ibid.* **16** (1960) 87.
5. G. BRAUER, K. A. GINGERICH and U. HOLTZSCHMIDT, *ibid.* **16** (1960) 77.
6. D. J. M. BEVAN and J. KORDIS, *ibid.* **26** (1964) 1509.
7. H. L. TULLER and A. S. NOWICK, *J. Electrochem. Soc.* **126** (1979) 209.

Received 5 June
and accepted 16 July 1980

G. T. BROWN
Royal Signals and Radar Establishment,
St Andrews Road,
Malvern, UK

I. R. HARRIS
Department of Physical Metallurgy,
Birmingham University,
Birmingham, UK